Functional neuroanatomy of biological motion perception in humans

Lucia M. Vaina, Jeffrey Solomon, Sanjida Chowdhury, Pawan Sinha, and John W. Belliveau

PNAS 2001;98;11656-11661; originally published online Sep 11, 2001;
doi:10.1073/pnas.191374198

Functional neuroanatomy of biological motion perception in humans

Lucia M. Vaina*†‡§¶, Jeffrey Solomon‖, Sanjida Chowdhury*, Pawan Sinha‡, and John W. Belliveau*§

*Boston University, Brain and Vision Research Laboratory, Department of Biomedical Engineering and Neurology, 44 Cummington Street, Boston, MA 02215; †Department of Neurology, Harvard Medical School, Boston, MA 02215; ‡Department of Cognitive Science, Massachusetts Institute of Technology, Cambridge, MA 02215; §Massachusetts General Hospital NMR Center, Building 149, 13th Streeet, Charlestown, MA 02129; and ‖Sensor Systems Inc., Sterling, VA 20164

Communicated by Charles G. Gross, Princeton University, Princeton, NJ, July 19, 2001 (received for review April 25, 2001)

We used whole brain functional MRI to investigate the neural network specifically engaged in the recognition of ''biological motion'' defined by point-lights attached to the major joints and head of a human walker. To examine the specificity of brain regions responsive to biological motion, brain activations obtained during a ''walker vs. non-walker'' discrimination task were compared with those elicited by two other tasks: (*i*) non-rigid motion (NRM), involving the discrimination of overall motion direction in the same ''point-lights'' display, and (*ii*) face-gender discrimination, involving the discrimination of gender in briefly presented photographs of men and women. Brain activity specific to ''biological motion'' recognition arose in the lateral cerebellum and in a region in the lateral occipital cortex presumably corresponding to the area KO previously shown to be particularly sensitive to kinetic contours. Additional areas significantly activated during the biological motion recognition task involved both, dorsal and ventral extrastriate cortical regions. In the ventral regions both face-gender discrimination and biological motion recognition elicited activation in the lingual and fusiform gyri and in the Brodmann areas 22 and 38 in superior temporal sulcus (STS). Along the dorsal pathway, both biological motion recognition and non-rigid direction discrimination gave rise to strong responses in several known motion sensitive areas. These included Brodmann areas 19/37, the inferior (Brodmann Area 39), and superior parietal lobule (Brodmann Area 7). Thus, we conjecture that, whereas face (and form) stimuli activate primarily the ventral system and motion stimuli primarily the dorsal system, recognition of biological motion stimuli may activate both systems as well as their confluence in STS. This hypothesis is consistent with our findings in stroke patients, with unilateral brain lesions involving at least one of these areas, who, although correctly reporting the direction of the point-light walker, fail on the biological motion task.

An intriguing perceptual phenomenon is that only a few lights attached to the head and the major limb-joints of an otherwise invisible human actor immediately allows adult observers to recognize that the moving ''light-points'' portray a person performing familiar actions. The form of the human actor remains obscure when the display is static or even when the light-points translate without any relative movement. In these cases, the pattern of lights gives no clue as to the cause of the lights: i.e., their global identity or the activities concerned. This illusion was termed by Johansson (1) ''biological motion'' (BM). Notwithstanding the absence of explicit contours linking joints, observers quickly identify the specific actions performed by a human actor, such as running, riding a bicycle, dancing, or shaking hands.

What neural substrates underlie the perception of BM? Single neurons in the superior temporal polysensory area (STP) in the superior temporal sulcus (STS) have been reported to be specifically sensitive to BM (2, 3). STP receives projections from the anterior parts of the dorsal and ventral visual streams, and we suggest that this area is the site of their synthesis (4). The dorsal stream may be further subdivided into at least two major substreams (5–7). One such substream, specialized for spatial and visuo-spatial functions, consists of visual areas V2, V3A, and PO and then areas 7 and adjacent intraparietal areas. Another substream, specialized for the analysis of complex motions, includes MT, MST, and FST and terminates in STP in the superior temporal sulcus (STS). Area STS also receives inputs from the inferior temporal cortex (5), an area crucial for object recognition (8–16). Furthermore, neurons in STS show remarkable selectivity for faces (17). We suggest that STS, and STP in particular, is in a position to integrate motion information from the dorsal system and object information from the ventral system.

This suggestion is supported by several behavioral studies of neurological cases. Patients with normal sensitivity to motion speed, direction, and pattern, may fail to perceive BM (18). Unexpectedly, patients with bilateral lesions along the dorsal pathway involving the human homologue of MT, such as patients LM (19) and AF (20), who were impaired on many aspects of visual motion perception to the extent that they are referred to as almost or completely ''motion-blind,'' can reliably recognize human actions in point-light displays. Because the human analogue of the macaque area MT/V5 was involved in these patients' lesions, their remaining dorsal pathway had limited access to STS and in particular to STP. Similarly surprising, patient EW, with bilateral ventral lesions involving the posterior temporal lobes (21), suffered from prosopagnosia and object agnosia, but could easily and correctly recognize BM. Thus, inputs from the ventral pathway to STP were not fully available, and we suggest that this patient mostly relied on the dorsal pathway. None of these patients had lesions involving the middle and anterior portion of STS (Brodmann areas 38 and 22). However, patients with lesions mainly affecting this region (unpublished data) were unable to recognize the simplest BM displays, although several other aspects of motion perception and object and face recognition were normal, as was their ability to discriminate the overall direction of the dynamic point-light clusters.

Thus, we conjecture that, whereas form and face stimuli activate primarily the ventral system and motion stimuli primarily the dorsal system, recognition of BM stimuli may activate both systems as well as their confluence in STP. We examined this possibility in normal human subjects, by using functional MRI (fMRI). We also examined the neuroanatomical substrates of the striking dissociation noted in neurological patients between preserved ability to discriminate the direction of the point-light display and the impaired recognition of the pattern of lights as a walker.

Abbreviations: BM, biological motion; STP, superior temporal polysensory area; STS, superior temporal sulcus; fMRI, functional MRI; NRM, non-rigid motion; STG, superior temporal gyrus.

¶To whom reprint requests should be addressed. E-mail: vaina@engc.bu.edu.

The publication costs of this article were defrayed in part by page charge payment. This article must therefore be hereby marked "*advertisement*" in accordance with 18 U.S.C. §1734 solely to indicate this fact.

 www.pnas.org/cgi/doi/10.1073/pnas.191374198

By using a blocked experimental design, we measured the blood oxygenation level-dependent (BOLD) fMRI response during the discrimination of a walker from a scrambled walker in a point-light display (Exp. 1, BM), discrimination of the overall motion direction of the stimuli used in Exp. 1 (Exp. 2, non-rigid motion), and a face-gender discrimination task (Exp. 3, face discrimination). The stimuli in Exps. 1 and 2 employ displays composed of discrete elements (point-lights) that represent the major joints and head of an otherwise invisible person walking as if on a treadmill or, in the case of the distractors, spatially scrambled versions of the walker. The actual motion in the point-lights displays (Exps. 1 and 2) portrays ± 30% of one walking cycle and is locally "non-rigid" (because the limbs oscillate around a central vertical axis but the adjacent limbs move in opposite directions). The "scrambled walker" was obtained by perturbing by random amounts the *x* or *y* position of the dots defining the walker, yet maintaining the same overall spatial extent of the entire group of dots. In the direction discrimination task, the observer must integrate the local motions of the dots and extract their coherent overall direction, left or right. In Exps. 1 (BM) and 2 (NRM), we presented observers with the same stimuli; what varied between the two experiments was the task. In one condition, BM, the observers' task was to discriminate whether the point-light display represented a man, whereas, in the other condition, NRM, they were asked to solely discriminate the overall direction of the non-rigid motion of the cluster of dynamic dots in the point-light display.

Methods

Three visual discrimination tasks were conducted on five naive right-handed volunteers (three males and two females, mean age 22.6, range 21–23 years). All subjects were neurologically healthy and had normal or corrected to normal (contact lenses) vision. All subjects gave their informed consent for the experimental protocol approved by the Massachusetts General Hospital Human Subjects Committee. Each subject participated in one imaging session. Subjects were scanned on a 1.5-tesla GE Signa MRI system, retrofitted for echo planar imaging (EPI; Instascan; Advanced NMR Systems, Wilmington, MA), by using a standard rf head coil. Details of scanning procedure are described in (22, 23). A conventional volume was acquired by using twenty 6-mm-thick contiguous oblique slices (3.125 mm × 3.125 mm in plane) parallel to a line drawn between the anterior and posterior commissure (AC-PC), sufficient to cover the whole brain. A flow series was obtained in the oblique planes selected for functional scanning to detect major blood vessels, followed by a T1-weighted sagittal localizer series [repetition time (TR) = 25 s, inversion time (TI) = 70 ms, NEX = 1, field of vision (FOV) = 24 cm, matrix 256 × 192]. These scans were used to guide slice selection for the functional acquisitions. Functional images, sensitive to changes in blood oxygenation state (BOLD), were obtained by using an ASE pulse sequence (TR = 2.5 s, TE = 70 ms, tau offset = 25 ms, 100 images per slice). For each subject, a high-resolution conventional structural scan (124-slice sagittal volume) was also acquired (SPGR:FOV = 24 cm, acquisition matrix 256 × 192, voxel size 1 × 1 × 1.5 mm, TE = 4 ms, TR = 25 ms).

Before entering the MRI chamber, subjects were fitted with earplugs. Subjects lay supine, foam pads were tightly put around the ears to hold the head still, and an adjustable bite-bar minimized head motion. Visual stimuli were computer generated and rear-projected onto an acrylic screen (Da-Lite Screen Company, Warsaw, IN) positioned at the head of the bore 40 cm from the subject. The screen provided an activated visual field up to 40° × 25°. Stimuli were projected through a collimating lens (Buhl Optical, Pittsburgh, PA) onto the screen by a magnetically shielded Sharp 2000 color LCD projector (Mahwan, NJ) with a screen resolution of 640 × 480 pixels. Subjects viewed the screen via a mirror. In each 240-s fMRI run, the subjects actively performed the discrimination task by entering their responses on a keypad connected to the computer, which was also used for data collection. Each experiment was repeated four times within the same scanning session. Synchronization of the stimulus presentation with the MR data acquisition was realized by starting the computer displays at the same time as the scanner.

Experimental Paradigm. All three experiments used an A-B-A design. In A, the baseline, subjects viewed a 60-s-long sequence consisting of a small cross fixation mark in the center of the display and turning randomly to the letters T or L briefly flashed (30 ms). Subjects were required to perform the letter discrimination. The baseline condition was identical in all three experiments. This letter discrimination task was chosen to reinforce fixation and control for sustained attention. In B, the task, subjects viewed for 120 s a sequence of stimuli each presented for 200 ms. Throughout a run, subjects were instructed to lie still, fixate on a cross displayed at the center of the stimulus, attend to the specific task they were asked to perform, and respond as soon as the stimulus disappeared. In all experiments, each trial (stimulus and response) lasted 1 s; thus, each run contained 120 stimuli. The displays in Exps. 1 and 2 consisted of 12 computer-generated bright white dots, each subtending 8.8 arcmin in diameter and moving at 3°/s. The movement and spatial arrangement of the dots representing the "walker" in Exps. 1 and 2 were generated by an algorithm adapted from Cutting (24). In both experiments, the spatial distribution and motion of the dots portrayed either a "walker" or a "scrambled walker," which resulted from randomly shifting within the body space the *x* and *y* coordinates of each light point, but maintaining its direction and speed. The display in Exp. 2 [non-rigid motion (NRM)] was identical to that in Exp. 1, but here subjects were required to discriminate only the overall direction of the NRM of the dots in the display. In Exp. 3 (FG) subjects were required to make a face-gender discrimination of black and white front view of faces of women and men presented in random order.

In all three experiments for both the A and B conditions, subjects performed a two-alternatives forced choice discrimination (2AFC) task, and all of the responses were given by pressing one of the two assigned buttons on a keypad. Both the sequence of stimuli and the order of the runs were randomized. Subjects' responses were viewed online, and a score on the baseline (A condition) of less than 95% correct was considered as indicative that the subject did not pay attention; therefore, that run was discarded. In all of the runs across all subjects, the performance on the baseline task was above 95% correct. Subjects' performance on the three discrimination tasks (BM, Faces, and NRM) varied between 94 and 96% correct, indicating that subjects were attentive and able to perform the tasks correctly. An ANOVA performed on the reaction time data indicated that there was no difference in subjects' performance among the three tasks ($F(2,12) = 0.053$, $P = 0.949$).

Data Analysis. Time-dependent echoplanar images were postprocessed by using the MEDX 3.1 software (Sensor Systems, Sterling, VA). Following head motion correction by using a method described in Woods *et al.* (25), to improve the signal-to-noise ratio, the time series was spatially smoothed with a Gaussian filter whose full width at half maximum (FWHM) was two times the voxel size in all three dimensions. Only voxels with values greater than 15% of the maximum intensity were used in the computation of the volume mean. To remove any linear drift in signal intensity, an estimate for linear trend was made for each voxel, and this trend was then removed from the time series data. The first six images of each run were excluded from analysis.

Planned contrasts between each of the motion and face discrimination conditions were computed by using the unpaired

Table 1. Talairach coordinates and *Z* scores for peak voxels in regions showing differential responses to BM, NRM, and face-gender discrimination

Area	Task	*x*	*y*	*z*	*Z* scores	Extent	Frequency
BA 19/37 (hMT+)	BM	42	−68	6	15.5304	2 to 8	5/5
	BM	−46	−68	6	7.924	4 to 8	5/5
	NRM	40	−66	6	12.939	2 to 8	5/5
	NRM	−44	−68	6	5.4164	2 to 8	4/5
Cuneus (BA 17/18)	BM	6	−94	12	8.5453	10 to 14	5/5
	BM	−22	−84	24	7.0084	22 to 26	5/5
	NRM	−20	−84	18	8.526	12 to 20	5/5
	NRM	20	−84	18	10.1154	18 to 24	5/5
	Face-gender	16	−86	8	9.7839	6 to 8	5/5
	Face-gender	−18	−90	4	9.3857	−2 to 8	5/5
Precuneus (BA 31)	BM	22	−78	26	9.7360	18 to 28	5/5
	NRM	24	−78	26	11.453	18 to 28	5/5
	Face-gender	22	−76	26	5.1360	18 to 28	5/5
Parieto-occipital junction	BM	20	−74	28	3.559	28 to 32	4/5
	NRM	20	−74	28	4.473	28 to 30	4/5
	Face-gender	22	−74	28	5.195	28	3/5
Lingual gyrus (BA 17/18)	BM	14	−92	0	9.0497	−2 to 2	5/5
	BM	−22	−74	−10	8.7805	−10 to −4	5/5
	NRM	20	−70	−4	6.9867	−10 to 4	5/5
	NRM	−20	−74	−6	9.2601	−10 to −2	5/5
	Face-gender	10	−88	4	8.9945	4 to 10	5/5
	Face-gender	−16	−90	−2	10.951	−4 to 2	4/5
Fusiform gyrus	BM	22	−64	−8	9.9281	−10 to −8	5/5
	BM	−26	−74	−14	8.1048	−14 to −12	5/5
	NRM	44	−62	−12	5.8332	−16 to −12	5/5
	Face-gender	28	−44	−12	7.923	−14 to −12	5/5
	Face-gender	−38	−52	−12	4.755	−16 to −12	5/5
Parahippocampal gyrus	BM	−28	−14	−22	6.0268	−26 to −22	4/5
	Face-gender	24	−46	−10	8.3711	−12 to −16	5/5
Ventral extrastriate cortex (KO)	BM	−32	−86	2	3.183	−1 to 4	4/5
	BM	28	−84	0	4.6874	−1 to 4	4/5
Superior temporal gyrus (BA 22)	BM	−46	−14	−6	4.2182	−6 to −2	4/5
	NRM	42	−56	14	3.5652	4	5/5
	Face-gender	54	−44	10	4.7750	6 to 12	5/5
Superior temporal gyrus (BA 38)	BM	−60	−12	−12	3.7339	−20 to −10	5/5
	Face-gender	−50	12	−26	4.8541	−30 to −16	5/5
BA 39	BM	44	−68	10	9.5248	10 to 12	5/5
	BM	−46	−74	10	7.8171	10 to 12	4/5
	NRM	46	−66	10	6.0717	10 to 20	5/5
BA 7	BM	22	−78	30	8.2940	30 to 60	4/5
	BM	−22	−78	30	9.0795	30 to 56	4/5
	NRM	24	−78	30	9.309	30 to 38	5/5
	NRM	−24	−78	30	7.4054	30 to 38	5/5
Cerebellum (QuP)	BM	−38	−66	−16	8.451	−18 to −8	5/5
	BM	−6	−78	−20	6.558	−22 to −12	5/5

Coordinates are in the normalized space of Talairach and Tournoux brain atlas (27). *N* indicates number of subjects in whom each region was identified according to our criteria (seven or more contiguous activated voxels).

t statistic (26). The parametric *t* statistic images for each contrast were then converted to the corresponding *z* map images by using a lookup table. These *z* map images were searched for local maxima, and the peak values were recorded. The time series for each peak voxel was examined to verify the presence of task-related signal intensity modulation. For neuroanatomical localization, for each run the *z* map parametric images were superimposed on the subject's high resolution MRI scan, which was normalized in the Talairach space (27). The steps required for this fusion of images are described in detail in Vaina *et al.* (28). For each contrast, the Talairach registered *z* score map images from all runs and subjects were summed and then divided by the square root of the total number of runs, providing a group *z* score map that was corrected for multiple comparisons (26). This correction constrained the thresholding value for the *z* maps. The method of developing a group *z* score map assumes the uniformity of noise across all of the image data used to create the *z* map images. For each condition, the combined *z* maps were thresholded at a *z* value of 4 and superimposed onto a subject's high resolution MRI in Talairach space. To differentiate levels of activation, the color display range used was red (minimum) to yellow (maximum). Talairach coordinates of peak activation were obtained by using the TALAIRACH DAEMON (http://ric.uthscsa.edu/projects/talairachdaemon.html), and the foci of activation found for each contrast in the group analysis are reported in Table 1. To determine activation areas unique to BM, the *z* map images for each of three experimental conditions were summed, and then the subtraction of ((BM − NRM) − FG)

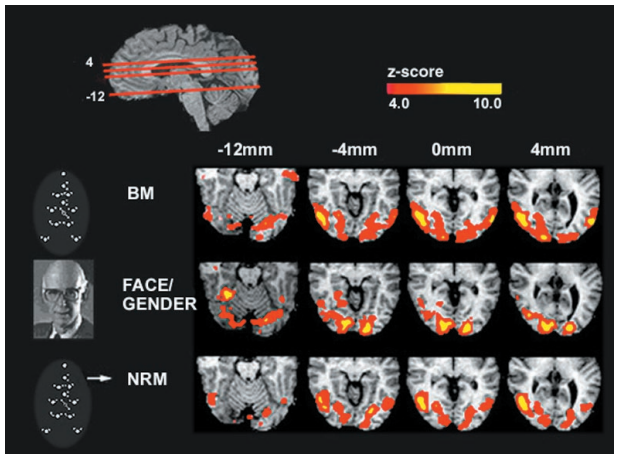

Fig. 1. Comparison of activity across the three experiments. The red lines through the top sagittal slice indicate the position of the axial slices in the figure. A schematic of the three stimuli used is shown on the left. On the right are displayed correlated group *z* maps showing statistically significant neural activity for each experiment. To generate these *z* maps for each experiment, a *t* test was performed to contrast each experiment's task with the control (letter discrimination at fixation). Results from individual subjects were combined to generate group results (see data analysis). The color scale represents the *z* score of the activation ($4 < z < 10$). The figure illustrates bilateral activations in the lingual and fusiform gyri in all three tasks. The Face-Gender (FG) discrimination task produces significantly stronger activity in these areas than the other two tasks, and BM had stronger activation than NRM (see Table 1). BM and NRM produce selectively strong activation in the hMT+ and the cuneus, and these areas are not significantly activated on the face-gender discrimination task (Table 1).

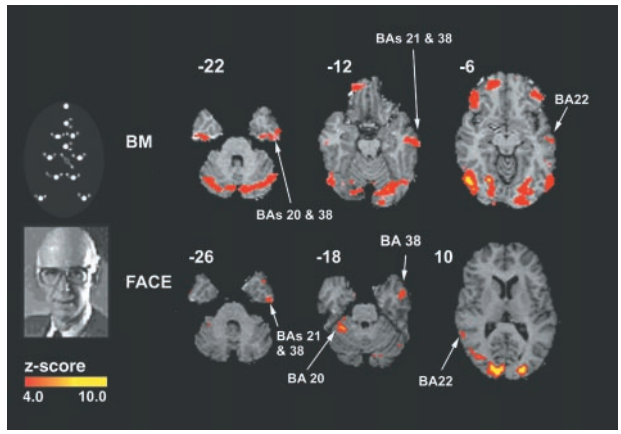

Fig. 2. Brain activity selective to biological motion and faces: emphasis on ventral stream. A schematic of the BM and face-gender (FG) discrimination stimuli used is shown on the left. On the right are displayed correlated group *z* maps showing statistically significant neural activity for each experiment. To generate these *z* maps for each experiment, a *t* test was performed to contrast each experiment's task with the control. Results from individual subjects were combined to generate group results (see *Data Analysis*). The color scale represents the *z* score of the activation ($4 < z < 10$). The figure shows that BM and face-gender tasks produce activations in the STG and BA 22 and 38. This finding supports the hypothesis that the ventral pathway is involved in both tasks.

was performed after each of the tasks was contrasted with the baseline. The result of this subtraction was divided by the square root of the total number of *z* map images used. This method was used to assess condition differences within individual subjects as well as within the group of subjects.

Results and Discussion

The anatomical localization of the activated cortical regions was done on the basis of the published ranges of Talaraich coordinates for the different areas and known anatomical landmarks. Fig. 1 illustrates averaged activity maps for all five subjects in the stereotaxic space of Talairach and Tournoux (27) for each of the three experimental tasks: BM, FG, and NRM, each contrasted with the baseline. Several clusters were identified across tasks, and Table 1 lists the Talairach coordinates and the *z* maps of the peak activations of these areas. Both the BM and NRM tasks strongly activated a region in the ventral lateral occipital cortex (Brodmann areas 19/37), which involves the hMT+ (22, 29–32) and the cuneus. The activity in the cuneus was centered on an area corresponding to the human cortical area V3A (33), with the most intense activity seen in the BM task (−22, −84, +24). These areas were not prominently activated in the face discrimination task (Exp. 3).

Intense activity during FG occurred in the middle posterior fusiform gyrus and the lingual gyrus, which is consistent with specific-face activation areas reported by a large number of functional imaging studies of face perception (23, 34–38). However, strong responses in the fusiform and lingual gyri were also elicited by the BM discrimination task and to a lesser extent by the NRM discrimination task.

In addition to the activation in the fusiform gyrus for both the FG and BM discrimination tasks, support for the hypothesis that the ventral pathway is involved in both tasks is illustrated in Fig. 2. The contrasts performed were between BM and baseline and between FG and baseline. Strong activation during both BM and FG discriminations was observed in the inferior, middle, and superior temporal gyri, roughly corresponding to BA 20, 21, 22, and 38. The BA 38 is a region in the superior temporal gyrus (STG) presumably corresponding to the human analogue of the monkey area STP (3, 39, 40). No activation in BA 38 was seen during the non-rigid direction discrimination task (NRM). Bilateral activation of STG selective to BM (41) was also reported in an fMRI study that contrasted activity during observation of a point-light display portraying a man running with a display of just random motion. The STG region was also activated in a positron-emission tomography (PET) study of visual perception of biologically possible motion contrasted with biologically impossible motion (42).

Fig. 3 illustrates areas of activation along the dorsal pathway, common to the BM and NRM motion tasks but not to the FG task. The contrasts performed were again between baseline and either BM or NRM. As shown in Fig. 1, the strongest activity was in hMT+. The direction discrimination of the point-light walker is a directionally complex locally non-rigid task. To perform it, subjects must discriminate the overall direction of the non-rigid motion pattern of the walker while walking left or right on a treadmill. When subjects are asked to discriminate the point-light walker from a non-walker (the dots still move left or right), the task involves figural recognition. Significant overlap of activation for these two tasks was found in the medial occipital and temporal gyri.

Fig. 4*A* shows activation specific only to the BM task in the lateral occipital cortex, a region corresponding to the area KO (Table 1) described as selective to kinetic boundaries (30, 43, 44). We suggest that, in the BM stimulus, kinetic boundaries (corresponding to the structure of the point-light walker) resulted from the integration of the differences in local direction of point-light motions with the goal of determining whether these together constitute the outline of a human silhouette walking. This area might correspond to the motion-defined objects area V3B (45).

Recently, it has been reported that the lateral occipital cortex and, thus, probably KO are activated by small kinetic stimuli (like the ones presented here) with or without a contour present.

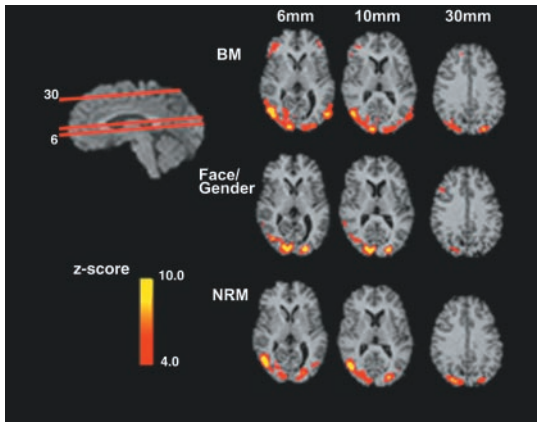

Fig. 3. Brain Activity selective to BM and NRM: emphasis on dorsal stream. The red lines through the sagittal slice (upper left) indicate the position of the axial slices in the figure. On the right are displayed group *z* maps showing statistically significant neural activity for each experiment (BM, face-gender, and NRM). To generate these *z* maps for each experiment, a *t* test was performed to contrast each experiment's task with the control. Results from individual subjects were combined to generate group results (see *Data Analysis*). The color scale represents the *z* score of the activation ($4 < z < 10$). The slices corresponding to BM and NRM illustrate activity in the BA 37/19 including the hMT+, BA 39, and BA 7. This finding supports the hypothesis that activation in the dorsal pathway is common to the BM and NRM experiments but not the face-gender discrimination experiment.

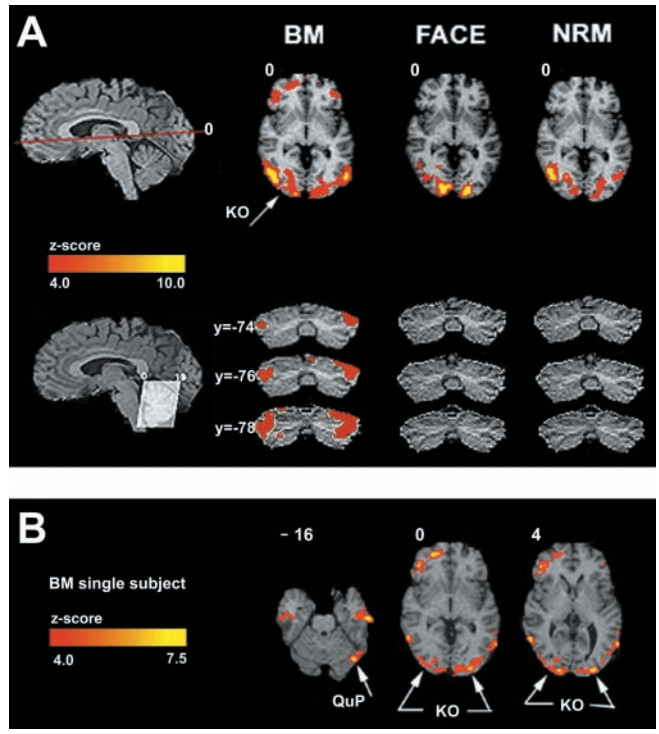

Fig. 4. Brain activity selective to BM. (*A*) The red line through the top sagittal slice indicates the position of the axial slice in the figure. On the upper right are displayed group *z* maps showing statistically significant neural activity for each experiment (BM, face-gender, and NRM). To generate these *z* maps for each experiment, a *t* test was performed to contrast each experiment's task with the control. Results from individual subjects were combined to generate group results (see *Data Analysis*). The color scale represents the *z* score of the activation ($4 < z < 10$). Bilateral activations selective to BM discrimination only were observed in KO ($x = 28$; $y = -84$, and $x = -28$; $y = -82$) and the lateral cerebellum. Mostly in the right hemisphere, the figure illustrates significant activation in the inferior frontal gyrus corresponding to BA47 ($x = 44$; $y = 20$). On the bottom left, the lines through the cerebellum in the sagittal slice indicate the angulation of the coronal cut. To the right, the three coronal slices (arranged vertically) show that only BM had activity in the lateral cerebellum. (*B*) Three axial slices illustrating activation for BM only (single subject). These slices illustrate activity is in KO, lateral cerebellum, and bilaterally in BA 21 (+54, −16, −16; −54, −16, −16) and in the right hemisphere activity in BA 38 (+54, +10, −16). To obtain this image, the sum of *z* maps from FG and from NRM were subtracted from the sum of *z* maps from BM and then divided by the square root of the total number of *z* maps. The resulting group *z* map, representing activation from BM only, was superimposed on the high resolution MRI in Talairach space.

However, when subjects performed the NRM discrimination task, the area KO was not activated. Therefore, we suggest that it is the task, not just the stimulus, that determines the activation areas. This hypothesis is further reinforced by the fact that BM discrimination produced only selective activation in the various areas of the cerebellum. As in previous studies of BM, we observed activity in the posterior lobe of the cerebellum (46) and in the anterior cerebellum, near the midline (47). Based on recent evidence from functional neuroimaging studies of the cerebellum in a variety of cognitive tasks, in particular in judgment of motor activity (48) or verb-generation (49) in response to visually presented nouns, Grossman (47) put forward an intriguing hypothesis. He suggested that, in the point-light walker displays, subjects might label the action portrayed in the BM sequence, thus reproducing activation through cognitive channels. In our study, we found additional strong activity in the lateral cerebellum (Fig. 4 bottom) for the BM recognition task. We suggest that the integration of the non-rigidly moving dots into a recognizable form (a walker) requires visual spatial attention. This hypothesis is supported by the fact that the strongest cerebellar activation was found in the lateral cerebellum, the area QuPO (Table 1), which was previously shown to be selective for visual spatial attention (28, 50). This area of the cerebellum was activated only during the BM task. However, common to all three tasks, there was a distributed network of significant activity involving the anterior cingulate, the frontal eye field, and the superior parietal lobule. These areas have been reported to be involved in directed attention (51), which is necessary for performing all of the tasks in this study.

Significant activation selective to BM was also found in the right inferior frontal gyrus corresponding to BA 45 and 47 (shown in Fig. 4*A*), which were reported previously in positron-emission tomography studies as being selectively active in visual tasks comparing apparent physically possible and impossible human movements (42) and in tasks comparing meaningful human actions and observations of stationary (hands; ref. 52). Strong activation specific to BM recognition were found only in BA 21 and 38, area KO, and the lateral cerebellum. Fig. 4*B* illustrates these BM-specific activations in a single subject after contrasting (BM − NRM) − FG).

General Discussion. We investigated the specific neuronal substrate of BM perception by comparing brain activity elicited by BM discrimination (BM task), to activity corresponding to discrimination of overall direction of motion in the BM stimuli (NRM task), but without the requirement of processing BM and with face-gender discrimination (FG task). We found that, in the BM task, brain activation was distributed across several cortical areas within the dorsal and the ventral visual processing streams (Figs. 1, 2, and 3). It has been suggested that these streams converge in the STG, areas of STS including a region probably corresponding to the human homologue of the monkey STP. STP is also involved in face discrimination. Previous functional neuroimaging studies in normal human subjects demonstrated involvement of STS and probably STP in BM perception. Bonda *et al.* (46) in a positron-emission tomography study reported that

the lower bank of the right posterior STS was selectively activated for movements of human actors in point-lights displays. STS was also reported active while observers viewed animation sequences of eye and mouth movements (53) or viewed a video of a face silently mimicking pronunciation of numbers and while they repeated silently these numbers. In an fMRI study, Howard *et al.* (41) reported that optic flow and point-light BM displays activated discrete and distinct regions bilaterally in STS, an area which also responds to auditory stimuli. They suggest that this area (Talairach coordinates +43 −19 +12 (BA41) and −47 −26 +17 (BA 42) within STG may correspond to the human homologue of the macaque STP situated anterior to the hMT+. We did not find activation in these Brodmann areas in any of the three tasks, but strong and specific responses to BM and FG were observed in other regions of the STG and the BA 22 and 38.

The differences in brain activity between the BM and NRM tasks bring further support to the suggestion that the subject's "task," not just the visual display (the visual stimuli were identical in the BM and NRM tasks), strongly contributes to the pattern of activation (54). Fig. 4 *A* and *B* demonstrated that, in the BM only, subjects need to link the pattern of the dynamic point-lights to determine whether the dots portray a man or not. We suggest that, to accomplish this, they use spatial attention (mediated by the lateral cerebellum), which facilitates the spatial integration of the dots into the overall kinetic form of a walker. Subjects' self reports of their percept during the two tasks support this conjecture. When asked to describe what they saw in the BM display, all subjects reported that they had a vivid percept of a human-figure walking. However, none of the subjects detected the walker in the NRM task, although the stimuli in the two experiments were absolutely identical.

We thank Charlie Gross for inspiring this study, Sabine Kastner and Jose Maisog for useful suggestions on the text and the data analysis, and E. B. Des Roziers and K. O'Craven for help with preliminary data analysis. We thank Laura Hughes for help with the figures. L.M.V. and S.F.C. were supported by National Institutes of Health (NIH) Grant EY2-RO1-07861, and J.W.B. was supported by NIH Grant RO1 NS37462. The fMRI data were acquired at the NMR Research Center under NIH Regional Resource Grant P41-RR14075.

1. Johansson, G. (1973) *Percept. Psychophys.* **14,** 201–211.
2. Oram, M. W. & Perrett, D. I. (1994) *J. Cognit. Neurosci.* **6,** 99–116.
3. Bruce, C., Desimone, R. & Gross, C. G. (1981) *J. Neurophysiol.* **46,** 369–384.
4. Felleman, D. J. & Van Essen, D. C. (1991) *Cereb. Cortex* **1,** 1–47.
5. Boussaoud, D., Ungerleider, L. G. & Desimone, R. (1990) *J. Comp. Neurol.* **296,** 462–495.
6. Gross, C. G. & Graziano, M. (1995) *Neuroscientist* **1,** 43–50.
7. Graziano, M. & Gross, C. G. (1994) in *The Cognitive Neurosciences*, ed. Gazzaniga, M. (MIT Press, Cambridge MA), pp. 1021–1034.
8. Gochin, P. M., Colombo, M., Dorfman, G. A., Gerstein, G. L. & Gross, C. G. (1994) *J. Neurophysiol.* **71,** 2325–2337.
9. Gross, C. G. (1992) *Philos. Trans. R. Soc. London B* **335,** 3–10.
10. Tanaka, K., Saito, H.-a., Fukada, Y. & Moriya, M. (1991) *J. Neurophsyiol.* **66,** 170–189.
11. Gross, C. G., Rocha-Miranda, C. E. & Bender, D. B. (1972) *J. Neurophysiol.* **35,** 96–111.
12. Gross, C. G., Desimone, R., Albright, T. & Schwartz, E. (1984) in *Cortical Integrity*, ed. Reinoso-Suarez, F. & Aimone-Marsan, C. (Raven Press, New York), pp. 291–315.
13. Tanaka, K. (1996) *Annu. Rev. Neurosci.* **19,** 109–139.
14. Logothetis, N. K. & Sheinberg, D. L. (1996) *Annu. Rev. Neurosci.* **19,** 577–621.
15. Desimone, R., Albright, T., Gross, C. G. & Bruce, C. (1984) *J. Neurosci.* **4,** 2051–2062.
16. Perrett, D., Oram, M., Harries, M., Bevan, R., Hietanen, J., Benson, P. & Thomas, S. (1991) *Exp. Brain Res.* **86,** 159–173.
17. Perrett, D. I., Mistlin, A. J. & Chitty, A. J. (1987) *Trends Neurosci.* **10,** 358–364.
18. Schenk, T. & Zihl, J. (1997) *Neuropsychologia* **35,** 1299–1310.
19. McLeod, P., Dittrich, W., Driver, J., Perret, D. & Zihl, J. (1996) *Visual Cognit.* **3,** 363–391.
20. Vaina, L. M., LeMay, M., Bienfang, D. C., Choi, A. Y. & Nakayama, K. (1990) *Visual Neurosci.* **5,** 353–369.
21. Vaina, L. M. (1994) *Cereb. Cortex* **4,** 555–572.
22. Watson, J. D., Myers, R., Frackowiak, R. S., Hajnal, J. V., Woods, R. P., Mazziotta, J. C., Shipp, S. & Zeki, S. (1993) *Cereb. Cortex* **3,** 79–94.
23. Kanwisher, N., McDermott, J. & Chun, M. M. (1997) *J. Neurosci.* **17,** 4302–4311.
24. Cutting, J. E. (1978) *Behav. Res. Methods Instrum.* **10,** 91–94.
25. Woods, R. P., Mazziotta, J. C. & Cherry, S. R. (1993) *J. Comp. Assist. Tomogr.* **17,** 536–546.
26. Snedcor, G. W. & Cochran, W. C. (1980) *Statistical Methods* (Iowa State Univ. Press, Ames, IA).
27. Talairach, J. & Tournoux, P. (1988) *Co-Planar Stereotaxic Atlas of the Human Brain* (Thieme Medical Publishers, New York).
28. Vaina, L. M., Belliveau, J. W., Roziers, B. D. & Zeffiro, T. A. (1998) *Proc. Natl. Acad. Sci. USA* **95,** 12657–12662.
29. Tootell, R. B. H., Reppas, J. B., Kwong, K. K., Malach, R., Born, R. T., Brady, T. J., Rosen, B. R. & Belliveau, J. W. (1995) *J. Neurosci.* **15,** 3215–3230.
30. Sunaert, S., Van Hecke, P., Marchal, G. & Orban, G. A. (1999) *Exp. Brain Res.* **127,** 355–370.
31. Reppas, J. B., Niyogi, S., Dale, A. M., Sereno, M. I. & Tootell, R. B. (1997) *Nature (London)* **388,** 175–179.
32. Cheng, K., Fujita, H., Kanno, I., Mura, S. & Tanaka, K. (1995) *J. Neurophysiol.* **74,** 413–426.
33. Tootell, R. B., Mendola, J. D., Hadjikhani, N. K., Ledden, P. J., Liu, A. K., Reppas, J. B., Sereno, M. I. & Dale, A. M. (1997) *J. Neurosci.* **17,** 7060–7078.
34. Puce, A., Allison, T., Gore, J. C. & McCarthy, G. (1995) *J. Neurophysiol.* **74,** 1192–1199.
35. Haxby, J. V., Ungerleider, L. G., Horwitz, B., Maisog, J. M., Rapoport, S. I. & Grady, C. L. (1996) *Proc. Nat. Acad. Sci. USA* **93,** 922–927.
36. Kanwisher, N., Stanley, D. & Harris, A. (1999) *NeuroReport* **10,** 183–187.
37. Chao, L., Martin, A. & Haxby, J. (1999) *NeuroReport* **10,** 2945–2950.
38. Kuskowski, M. & Pardo, J. (1999) *NeuroImage* **9,** 599–610.
39. Perrett, D. I., Smith, P. A. J., Mistlin, A. J., Chitty, A. J., Head, A. S., Potter, D. D., Broennimann, R., Milner, A. D. & Jeeves, M. A. (1985) *Behav. Brain Res.* **16,** 153–170.
40. Hietanen, J. K. & Perrett, D. I. (1993) *Exp. Brain Res.* **93,** 117–128.
41. Howard, R. J., Brammer, M., Wright, I., Woodruff, P. W., Bullmore, E. T. & Zeki, S. (1996) *Curr. Biol.* **6,** 1015–1019.
42. Stevens, J., Fonlupt, P., Shiffrar, M. & Decety, J. (2000) *NeuroReport* **11,** 109–115.
43. Dupont, P., De Bruyn, B., Vandenberghe, R., Rosier, A., Michiels, J., Marchal, G., Mortelmans, L. & Orban, G. A. (1997) *Cereb. Cortex* **7,** 283–292.
44. Van Oostende, S., Sunaert, S., Van Hecke, P., Marchal, G. & Orban, G. (1997) *Cereb. Cortex* **7,** 690–701.
45. Malach, R., Reppas, J. B., Benson, R. R., Kwong, K. K., Jiang, H., Kennedy, W. A., Ledden, P. J., Brady, T. J., Rosen, B. R. & Tootell, R. B. H. (1995) *Proc. Natl. Acad. Sci. USA* **92,** 8135–8139.
46. Bonda, E., Petrides, M., Ostry, D. & Evans, A. (1996) *J. Neurosci.* **16,** 3737–3744.
47. Grossman, E., Donnelly, M., Price, R., Pickens, D., Morgan, V., Neighbor, G. & Blake, R. (2000) *J. Cognit. Neurosci.* **12,** 711–720.
48. Fiez, J. (1996) *Neuron* **16,** 13–15.
49. Petersen, S., Fox, P., Posner, M., Mintun, M. & Raichle, M. (1989) *J. Cognit. Neurosci.* **1,** 153–170.
50. Allen, G., Buxton, R., Wong, E. & Courchesne, E. (1997) *Science* **275,** 1940–1943.
51. Kastner, S. & Ungerleider, L. (2000) *Annu. Rev. Neurosci.* **23,** 315–342.
52. Grezes, J., Costes, N. & Decety, J. (1998) *Cognit. Neuropsychol.* **15,** 553–582.
53. Puce, A., Allison, T., Bentin, S., Gore, J. C. & McCarthy, G. M. (1998) *J. Neurosci.* **18,** 2188–2199.
54. O'Craven, K. M., Rosen, B. R., Kwong, K. K., Treisman, A. & Savoy, R. L. (1997) *Neuron* **18,** 591–598.